Image based cardiac acceleration map using statistical shape and 3D+t myocardial tracking models; in-vitro study on heart phantom

Ali Pashaei, Gemma Piella, Xavier Planes, Nicolas Duchateau, Teresa María de Caralt, Marta Sitges, Alejandro Frangi

Image based cardiac acceleration map using statistical shape and 3D+t myocardial tracking models; in-vitro study on heart phantom

Ali Pashaei[a], Gemma Piella[a], Xavier Planes[a], Nicolas Duchateau[b], Teresa María de Caralt[b], Marta Sitges[b], and Alejandro F. Frangi[c]

[a]CISTIB, Universitat Pompeu Fabra, Barcelona, Spain;
[b]Hospital Clínic, IDIBAPS, Universitat de Barcelona, Barcelona, Spain;
[c]CISTIB, University of Sheffield, Sheffield, UK

ABSTRACT

It has been demonstrated that the acceleration signal has potential to monitor heart function and adaptively optimize Cardiac Resynchronization Therapy (CRT) systems. In this paper, we propose a non-invasive method for computing myocardial acceleration from 3D echocardiographic sequences. Displacement of the myocardium was estimated using a two-step approach: (1) 3D automatic segmentation of the myocardium at end-diastole using 3D Active Shape Models (ASM); (2) propagation of this segmentation along the sequence using non-rigid 3D+t image registration (temporal diffeomorphic free-form-deformation, TDFFD). Acceleration was obtained locally at each point of the myocardium from local displacement. The framework has been tested on images from a realistic physical heart phantom (DHP-01, Shelley Medical Imaging Technologies, London, ON, CA) in which the displacement of some control regions was known. Good correlation has been demonstrated between the estimated displacement function from the algorithms and the phantom setup. Due to the limited temporal resolution, the acceleration signals are sparse and highly noisy. The study suggests a non-invasive technique to measure the cardiac acceleration that may be used to improve the monitoring of cardiac mechanics and optimization of CRT.

Keywords: cardiac motion; acceleration measurement; statistical shape models; temporal image registration; cardiac phantom.

1. INTRODUCTION

Over the last years randomized clinical trials have tried to show the benefits of cardiac resynchronization therapy (CRT) to reduce mortality and morbidity in patients with congestive heart failure.[1] However, results have demonstrated that up to 30% of patients are non-responders to CRT[2] and that commonly used echocardiographic criteria cannot be recommended for patient selection and therapy optimization.[3] Mechanical indices for therapy optimization can also be obtained from either external sensors (seismocardiography) or implantable devices (peak endocardial acceleration) to measure myocardial contractility and hemodynamic heart function (max dp/dt).[4,5] More importantly they have been proposed as an optimization tool for CRT.[6,7] These indices are based on external or internal accelerometers that detect acceleration signals induced by the myocardium as a consequence of various mechanical forces that originate from myocardial contraction and blood flow at a single location.

Despite their high temporal sampling, accelerometers measure mechanical function locally, which might provide difficulties in the global characterization of cardiac dyssynchronies. Also it was indicated that accelerometer measurements are influenced by patient orientation and gravity.[8,9] Using medical images, in addition to the non-invasiveness of the method for computing myocardial acceleration, has the advantage of estimating this information at every location of the myocardium. However, their processing requires being able to accurately segment the cardiac anatomy and track it along the cardiac cycle.

Further author information: (Send correspondence to Ali Pashaei)
Ali Pashaei, Universitat Pompeu Fabra, 138 c/ Roc Boronat, 08018 Barcelona, Spain. E-mail: ali.pashaei@upf.edu

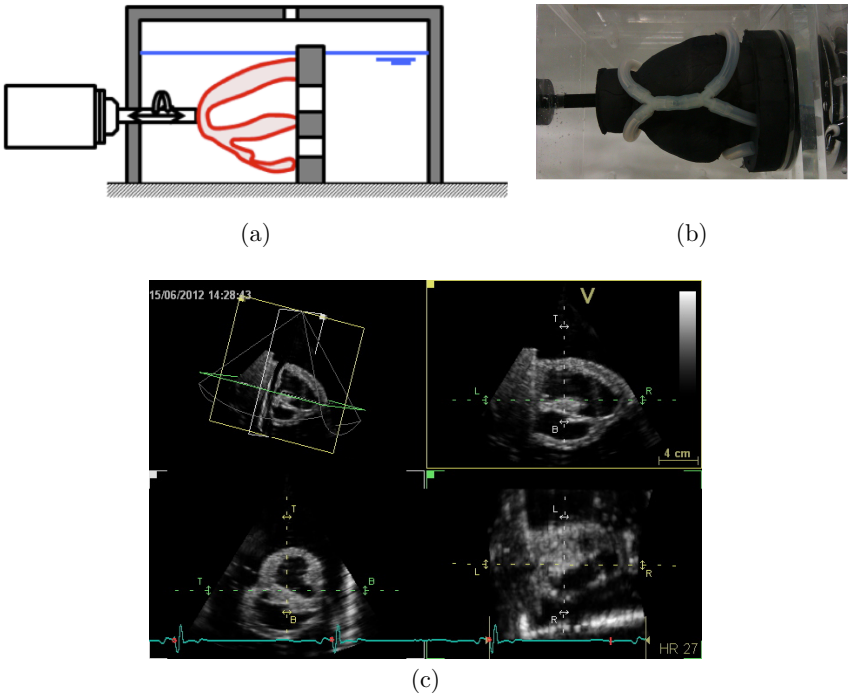

(a) (b)

(c)

Figure 1. The dynamic heart phantom and related experiments: (a) a schematic of the phantom structure, including biventricular heart phantom, its chamber and related control system, (b) a closer view of the biventricular heart phantom and (c) a snapshot of 2D orthogonal cuts from a 3D echocardiographic sequence of the phantom.

Automatic segmentation at a given instant of the cycle can be addressed by recent techniques such as Active Shape Models (ASM), where correspondence between the model and the studied subject is computed through volumetric elastic registration.[10] The resulting correspondence has been used for simulation of cardiac electrical and haemodynamical function.[11,12] Tracking along the cardiac cycle can be addressed by recently proposed algorithms such as temporal diffeomorphic free-form-deformation (TDFFD), which extends previous diffeomorphic FFD algorithms to 3D+t.[13] The algorithm provides rather smooth displacements, both in time and space, which may be an advantage for the estimation of acceleration (second temporal derivative of displacement). In this paper, we present the results achieved on a synthetic heart phantom with known ground truth for displacement at specific locations.

2. MATERIALS AND METHODS

2.1 Imaging data

A dynamic multimodality heart phantom (DHP-01, Shelley Medical Imaging Technologies, London, ON, CA) was employed to provide data for validation of the acceleration measurement from images. This phantom mimics realistic anatomical geometry of the left and right ventricles of the human heart. It has two controlable actuation systems to simulate the required myocardial deformation. The experimental phantom setup is shown in Fig.1. The study is repeated for two actuator configurations in which deformation of the myocardium follows linear and sinus wave form functions. All images were acquired with gating to a simulated vector ECG. Segmentation was performed at end-diastole. Acceleration was computed from 3D echocardiographic sequences (3DUS), and 2D sequences were used for ground truth checking directly from the images (using M-mode visualization). Temporal resolution was around 20 fps for 3D and $>$ 100 fps for 2D.

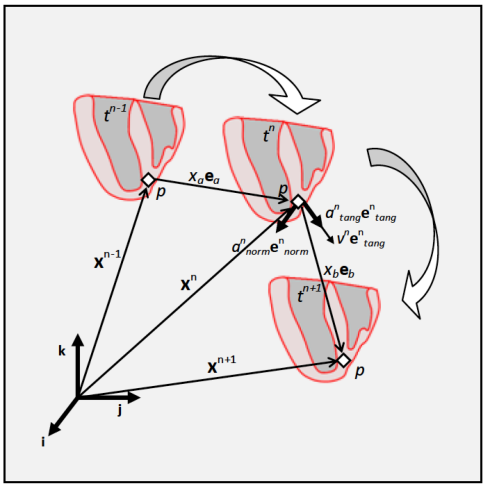

Figure 2. Reference and deformed configurations for computation of acceleration.

2.2 Deformation data

Segmentation of the left ventricle (LV) was first performed using 3D Active Shape Models (ASM).[14,15] The mesh resulting from the segmentation was matched to the 3DUS sequence and propagated along the cycle by means of a non-rigid image registration algorithm (TDFFD). With this segmentation-registration approach we can guarantee the anatomical correspondence of all points in the biventricular mesh. We used a two-level multiresolution implementation of the TDFFD, the initial grid size being of one control point per frame in the temporal direction, 5 control points in the short-axis direction and 3 control points in the long-axis direction. As similarity measure, we used the sum of squared differences between the intensities of each frame and a reference (end-diastole) one. We used the limited memory Broyden-Fletcher-Goldfarb-Shannon minimization with simple-bounds as optimizer (L-BFGS-B).[16] The output of the algorithm is a 3D+t displacement field, from which acceleration is computed further on. The LV was divided using the 17-segment model as proposed by the American Heart Association (AHA).[17]

2.3 Computation of acceleration

The displacement vector and time interval between image sequences were used to approximate the acceleration vector. Numerical differentiation was computed with a forward difference scheme for the first derivative to compute the velocity of the points. Fig.2 illustrates the reference and deformed configurations used to describe the formulation for computing acceleration. Consider a point p with position vector $\mathbf{x}^n$ at reference time t^n whose tracked position in time t^{n-1} and t^{n+1} is projected within the same coordinate system. Superscript n here indicates arbitrary time frame from image data. The displacement vector of this point is described by a scalar distance x and unit vector $\mathbf{e}$, indexed by a and b for deformed configurations before and after this time frame. The unit vectors for these displacement vectors are computed as below:

$$\mathbf{e}_a = \frac{\mathbf{x}^n - \mathbf{x}^{n-1}}{|\mathbf{x}^n - \mathbf{x}^{n-1}|}, \quad \text{and} \quad \mathbf{e}_b = \frac{\mathbf{x}^{n+1} - \mathbf{x}^n}{|\mathbf{x}^{n+1} - \mathbf{x}^n|}. \tag{1}$$

Assuming uniform sampling of the temporal sequences ($\Delta t = t_n - t_{n-1} = t_{n+1} - t_n$), the speed of point p in the reference time frame n will be obtained from:

$$v^n = \frac{v_a + v_b}{2}, \tag{2}$$

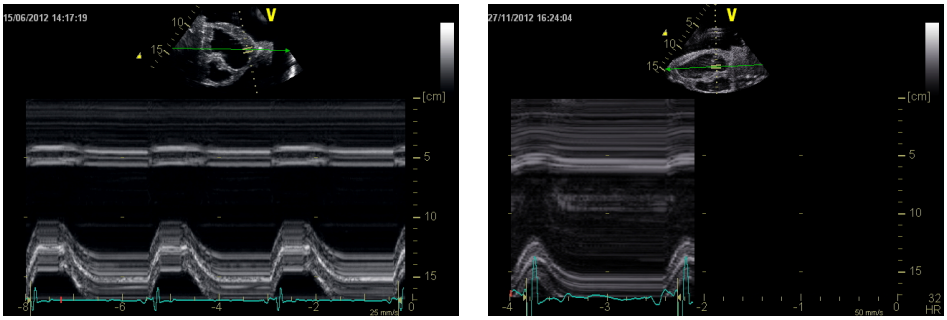

(a) (b)

Figure 3. 2D M-mode sequences used for estimating the ground truth deformation field for (a) linear and (b) sine wave form deformation of the phantom.

where speed values v_a and v_b are computed from distance and timing data as $\frac{|\mathbf{x}^n - \mathbf{x}^{n-1}|}{t^n - t^{n-1}}$ and $\frac{|\mathbf{x}^{n+1} - \mathbf{x}^n|}{t^{n+1} - t^n}$, respectively. Velocity vector is defined as multiplication of v^n to unit vector $\mathbf{e}^n_{tang}$ which is tangent to the point trace over time. Acceleration is the time rate of change of velocity vector, $\frac{d(v^n \mathbf{e}^n_{tang})}{dt}$. In the expanded form this derivative will be:

$$\mathbf{a}^n = \frac{dv^n}{dt}\mathbf{e}^n_{tang} + v^n \frac{d\mathbf{e}^n_{tang}}{dt}, \tag{3}$$

and discretized as

$$\mathbf{a}^n = \frac{v_b - v_a}{\Delta t}\mathbf{e}^n_{tang} + v^n \frac{|\mathbf{e}_b - \mathbf{e}_a|}{\Delta t}\mathbf{e}^n_{norm}. \tag{4}$$

Therefore, the acceleration vector is composed of two perpendicular components: $\mathbf{e}^n_{tang}$ which is tangent to the trajectory of the point and $\mathbf{e}^n_{norm}$ is normal to this trajectory (in the direction that unit tangent vector rotates). The following definitions for the unit vectors are used:

$$\mathbf{e}^n_{tang} = \frac{\mathbf{e}_a + \mathbf{e}_b}{|\mathbf{e}_a + \mathbf{e}_b|}, \quad \text{and} \quad \mathbf{e}^n_{norm} = \frac{\mathbf{e}_b - \mathbf{e}_a}{|\mathbf{e}_b - \mathbf{e}_a|}. \tag{5}$$

Using these unit vectors, the acceleration vector can further be projected onto a local cardiac coordinate system to obtain the acceleration in the radial, circumferential and longitudinal directions. These directions are defined on the mesh obtained from segmenting the LV. Computation was repeated for all nodes in all time frames. Data for the first and last frames were computed under periodicity assumption (therefore implying the last and first frames, respectively).

3. RESULTS

3.1 Ground truth

2DUS sequences were used to estimate the ground truth displacement magnitude directly from images. This is performed at the apex location, as actuators are connected to the apex, and the displacement visible on the images directly relates to the actuator displacement. This process was realized for both linear and sinus waveforms, as presented in Fig.3. The peak of displacement for the linear and sinus deformation is about 30 ± 1 mm, which is close to 28.5 mm, the setting for the stroke of the actuator in the phantom as used in the program.

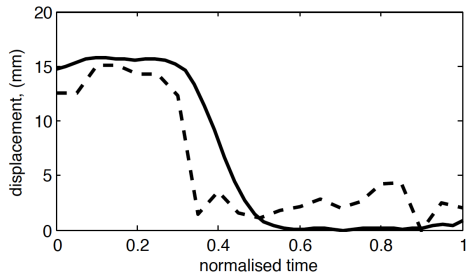

Figure 4. Left ventricular apex displacement vector magnitude along one cardiac cycle given from manual segmentation (solid line), and TDFFD algorithm (dashed line) for the linear displacement programming.

3.2 Local displacements

The displacement map is calculated for each node of the mesh, along the cardiac cycle. The first time frame corresponds to the end-diastolic phase. Fig.4 illustrates the recovered displacements magnitude at the apex (average over the 17th AHA segment), so that comparison with the 2D M-mode traces can be easily performed. For the linear waveform, results obtained with TDFFD are compared with the ones obtained with manual propagation of the ASM along the cycle, the latter being much noisier.

Fig.5 illustrates the recovered displacements magnitude at the apex using TDFFD and its comparison with an analytic sine wave function. TDFFD follows the configured displacement function, however comparison with M-mode shows that our image-based methods underestimates displacement magnitude.

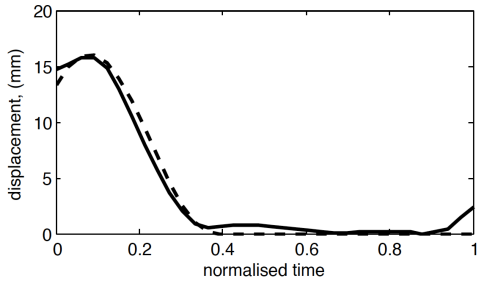

Figure 5. Left ventricular apex displacement along one cardiac cycle given from TDFFD algorithm (solid line) compared to an analytic sinus wave (dashed line). The TDFFD algorithm accurately follows the sine wave function, which is used for phantom configuration.

3.3 Local acceleration

Fig.6 shows the acceleration of apex for the case with sine wave form displacement. The acceleration curve presents some fluctuations due to the second order differentiation using a sparse number of time frames. The acceleration peak corresponds to the displacement peak that has the maximum deformation, resulting similar configuration as a sine wave as expected for the acceleration for apex. Fig.6(b) provides the projection of the acceleration wave along the radial direction in the apex, presenting even less noise in the curve.

3.4 Acceleration map

Fig.7 shows the distribution of the acceleration map at different phases during heart cycle. In general apex region has the highest acceleration at different time frames, while lower values are observed for the basal level. The maximum acceleration distribution is observed in time 0 and time 1, when higher values of acceleration observed. Over the cycle, we obtained a rather smooth change on the spatial distribution.

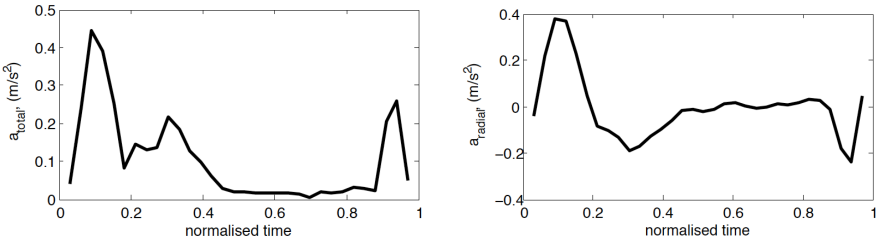

(a) (b)

Figure 6. Acceleration of Left ventricular apex for the sine wave: (a) magnitude of computed acceleration vector and, (b) its projection along the radial direction.

4. DISCUSSION

In this study, we have presented a method to compute myocardial acceleration from 3D image sequences. Computing myocardial acceleration from medical images has several advantages over other existing techniques: (1) the echocardiographic acquisition is non-invasive, and the invasiveness of the CT procedure could be overcome by directly segmenting echocardiographic data; (2) is less sensitive to environmental factors such as breath, sensor placement and gravity; (3) provides information at any location of the myocardium, and not a single one.

The results accuracy is highly conditioned by the temporal resolution, particularly critical in 3D, and source of noise for acceleration computations (second temporal derivative). Since the calculation of the acceleration depends on displacement fields obtained using ASM and TDFFD algorithms along heart cycle, imaging quality has a significant role.

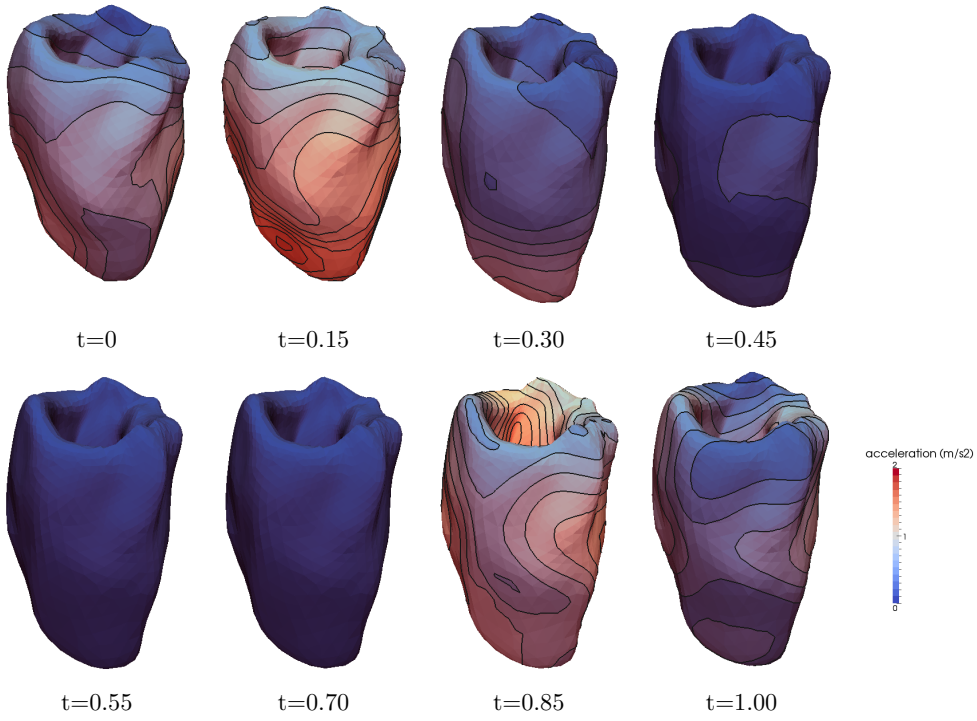

Figure 7. Spatial distribution of the acceleration map during the heart cycle over normalised time. Units in $m.sec^{-2}$.

Note that the technique is not specific to 3D echocardiography and could be applied to any imaging modality, provided its quality and spatiotemporal resolution are enough. Further extension of the method will consist in its application to real patient data.

5. CONCLUSION

We demonstrated the feasibility of the methodology for acceleration computations. An advantage of our method is the use of non-rigid registration algorithm to estimate smooth myocardial velocities, thus obtaining a less noisy acceleration. Good correlation has been demonstrated between the displacement field computed from using construction of shape model and phantom setup. Due to the low number of time frames, the acceleration signals of points are sparse. The study suggests a non-invasive technique to measuring the cardiac acceleration that might be used to improve the monitoring of cardiac mechanics and optimization of CRT.

ACKNOWLEDGMENTS

This work has been partially funded by the European Commission (FP7-ICT-2007-224485) under the euHeart project and by the Spanish Ministry of Science and Innovation under the cvREMOD CENIT Project (CEN20091044 and TIN2011-28067). Authors acknowledge the excellent assistance from Catalina Tobon-Gomez (KCL, London, UK), David Flores, Adelina Doltra and Luigi Gabrielli (Hospital Clínic, Barcelona, Spain) during image acquisition.

REFERENCES

[1] Cleland, J. G., Daubert, J. C., Erdmann, E., Freemantle, N., Gras, D., Kappenberger, L., Tavazzi, L., and Cardiac Resynchronization-Heart Failure (CARE-HF) Study Investigators, "The effect of cardiac resynchronization on morbidity and mortality in heart failure," *N Engl J Med* **352**(15), 1539–1549 (2005).

[2] Ismail, H. and Makaryus, A., "Predictors of response to cardiac resynchronization therapy: the holy grail of electrophysiology," *The International Journal of Cardiovascular Imaging (formerly Cardiac Imaging)* **26**(2), 197–198 (2010).

[3] Chung, E. S., Leon, A. R., Tavazzi, L., Sun, J. P., Nihoyannopoulos, P., Merlino, J., Abraham, W. T., Ghio, S., Leclercq, C., Bax, J. J., Yu, C. M., Gorcsan, J., St John Sutton, M., De Sutter, J., and Murillo, J., "Results of the predictors of response to crt (prospect) trial," *Circulation* **117**(20), 2608–2616 (2008).

[4] Bordachar, P., Labrousse, L., Ploux, S., Thambo, J. B., Lafitte, S., Reant, P., Jais, P., Haissaguerre, M., Clementy, J., and Dos Santos, P., "Validation of a new noninvasive device for the monitoring of peak endocardial acceleration in pigs: implications for optimization of pacing site and configuration," *Journal of Cardiovascular Electrophysiology* **19**(7), 725–729 (2008).

[5] Halvorsen, P. S., Remme, E. W., Espinoza, A., Skulstad, H., Lundblad, R., Bergsland, J., Hoff, L., Imenes, K., Edvardsen, T., Elle, O. J., and Fosse, E., "Automatic real-time detection of myocardial ischemia by epicardial accelerometer," *J Thorac Cardiovasc Surg* **139**(4), 1026–1032 (2010).

[6] Delnoy, P. P., Marcelli, E., Oudeluttikhuis, H., Nicastia, D., Renesto, F., Cercenelli, L., and Plicchi, G., "Validation of a peak endocardial acceleration-based algorithm to optimize cardiac resynchronization: early clinical results," *Europace* **10**(7), 801–808 (2008).

[7] Olsen, N., Mogelvang, R., Jons, C., Fritz-Hansen, T., and Sogaard, P., "Predicting response to cardiac resynchronization therapy with cross-correlation analysis of myocardial systolic acceleration: a new approach to echocardiographic dyssynchrony evaluation," *Journal of the American Society of Echocardiography* **22**(6), 657–664 (2009).

[8] Remme, E., Hoff, L., Halvorsen, P., Opdahl, A., Fosse, E., and Elle, O., "Simulation model of cardiac three dimensional accelerometer measurements," *Medical Engineering and Physics* **34**(7), 990–998 (2012).

[9] Remme, E. W., Hoff, L., Halvorsen, P. S., Naerum, E., Skulstad, H., Fleischer, L. A., Elle, O. J., and Fosse, E., "Validation of cardiac accelerometer sensor measurements," *Physiological Measurement* **30**(12), 1429–1444 (2009).

[10] Frangi, A. F., Rueckert, D., Schnabel, J. A., and Niessen, W. J., "Automatic construction of multiple-object three-dimensional statistical shape models: application to cardiac modeling.," *IEEE Trans Med Imaging* **21**(9), 1151–1166 (2002).

[11] Pashaei, A., Hoogendoorn, C., Sebastian, R., Romero, D., Camara, O., and Frangi, A. F., "Effect of scar development on fast electrophysiological models of the human heart: In-silico study on atlas-based virtual populations," in [*Functional Imaging and Modeling of the Heart*], **6666**, 427–436 (2011).

[12] Moosavi, M. H., Fatouraee, N., Katoozian, H., Pashaei, A., Camara, O., and Frangi, A. F., "Numerical simulation of blood flow in the left ventricle and aortic sinus using magnetic resonance imaging and computational fluid dynamics," *Comput Methods Biomech Biomed Engin* (2012).

[13] De Craene, M., Piella, G., Camara, O., Duchateau, N., Silva, E., Doltra, A., D'hooge, J., Brugada, J., Sitges, M., and Frangi, A. F., "Temporal diffeomorphic free-form deformation: application to motion and strain estimation from 3d echocardiography," *Medical Image Analysis* **16**(2), 427–450 (2012).

[14] van Assen, H. C., Danilouchkine, M. G., Frangi, A. F., Ordas, S., Westenberg, J. J. M., Reiber, J. H. C., and Lelieveldt, B. P. F., "SPASM: a 3D-ASM for segmentation of sparse and arbitrarily oriented cardiac MRI data," *Medical Image Analysis* **10**(2), 286–303 (2006).

[15] Tobon-Gomez, C., Sukno, F., Butakoff, C., Huguet, M., and Frangi, A., "Automatic training and reliability estimation for 3d asm applied to cardiac mri segmentation," *Physics in Medicine and Biology* **57**(13), 4155 (2012).

[16] Byrd, R., Lu, P., Nocedal, J., and Zhu, C., "A limited memory algorithm for bound constrained optimization," *SIAM Journal on Scientific Computing* **16**(5), 1190–1208 (1995).

[17] Cerqueira, M., Weissman, N., Dilsizian, V., Jacobs, A., Kaul, S., Laskey, W., Pennell, D., Rumberger, J., Ryan, T., Verani, M., et al., "Standardized myocardial segmentation and nomenclature for tomographic imaging of the heart a statement for healthcare professionals from the cardiac imaging committee of the council on clinical cardiology of the american heart association," *Circulation* **105**(4), 539–542 (2002).